PRUSSIAN BLUE ANALOGS: ELECTROSYNTHESIS AND CHARACTERIZATION

Lezna[1], R.O.; de Tacconi[2], N.R.
[1]INIFTA, CONICET. Universidad Nacional de La Plata. C.C. 16, Suc. 4. La Plata, (B1906ZAA), Argentina
[2]Department of Chemistry and Biochemistry. The University of Texas at Arlington. Arlington, TX 76019-0065,US.
e-mail: rolezna@inifta.unlp.edu.ar

Received May 3, 2003. Accepted in Final Form June 30, 2003
Dedicated to Professor Dr. A.J. Arvia on occasion of his 75th Anniversary

Abstract

This article focuses on the electrodeposition and in situ characterization of Prussian blue analogs with the generic formula: $A_hM_k[Fe(CN)_6]_l.mH_2O$, where h, k, l, m are stoichiometric numbers, A = alkali metal cation, and M is a transitionmetal. Six such metal hexacyanoferrate (MHCF) compounds derived from Cu, Pd, In, V, Co and Ni are featured in this article. The electrodeposition of MHCF films on targeted substrates is discussed through data obtained by cyclic voltammetry and complementary techniques. In situ spectroelectrochemical characterization of these films in the infrared and UV-visible regions is then discussed and constitutes the main topic of this article.

Resumen

Este artículo trata de la caracterización in-situ de películas electrodepositadas de análogos del Azul de Prusia con la fórmula genérica: $A_hM_k[Fe(CN)_6]_l.mH_2O$, donde h, k, l, m son coeficientes estequiométricos, A es un catión de metal alcalino y M es un metal de transición. La presentación analiza seis hexacianoferratos metálicos (MHCF) derivados del Cu, Pd, In, V, Co y Ni. La electrodeposición de películas de MHCF sobre sustratos seleccionados, se discute primeramente mediante el análisis de datos obtenidos por voltametría cíclica con la ayuda de técnicas complementarias. La caracterización espectroelectroquímica in-situ de estas películas en las zonas espectrales IR y UV-Visible es luego analizada en detalle y constituye el tópico principal de este trabajo.

Introduction

Transition metal hexacyanoferrates of the general formula: $A_hM_k[Fe(CN)_6]_l.mH_2O$ (h, k, l, m = stoichiometric numbers, A = alkali metal cation, M = transition metal ion) (Table 1), represent an important class of mixed-valence compounds, of which Prussian blue or iron (III) hexacyanoferrate (II) (with A = K and M = Fe in the above generic formula) is the classical prototype. Aside from their interesting solid-state chemistry and structural attributes, these compounds have garnered intense recent interest because of their electrocatalytic, electrochromic, ion exchange, ion sensing, and photomagnetic properties. While the electrochemistry and applications of

Prussian blue itself have been rather extensively discussed (1,2), only recently have the other transition metal analogs begun to receive attention.

In this article, we present a comparative discussion of the growth and in situ characterization of the Cu, Pd, In, V, Co, and Ni analogs. Our choice of these particular compounds for this article is simply motivated by the burgeoning literature on their applications, and by our own interest in them. After a primer on their solid-state chemistry, the growth of thin films of these compounds on targeted substrates is briefly discussed. In situ post-deposition characterization of these films, mainly by spectroelectrochemical methods is in fact the main topic of this article.

The chemistry of mixed-valence compounds has been extensively discussed by previous authors (1-6). The structural aspects and electrochemistry of Prussian blue itself have been previously reviewed (7,8). Many of the compounds addressed in the present article, have been described in terms of their electrochromic properties (2). Finally, the magnetic properties of Prussian blue analogs have also been discussed (9). Every attempt has been made to avoid redundancy between these earlier treatments and the present article, while unavoidable areas of overlap will be highlighted in what follows.

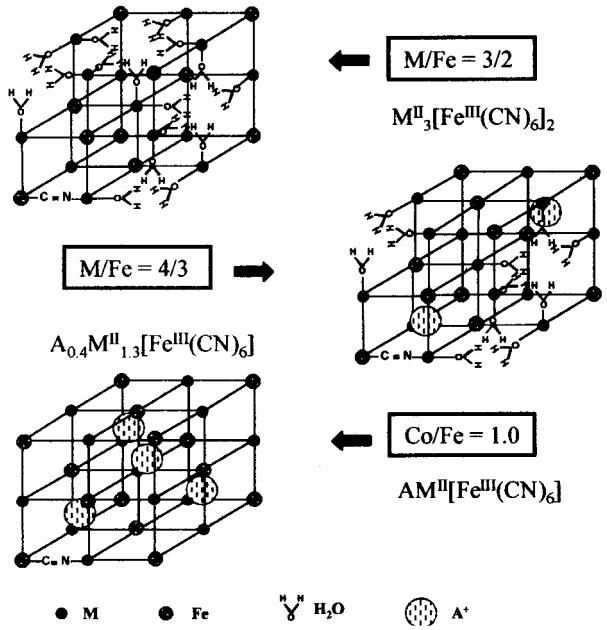

***Figure 1**:Unit cell representation of $M_3[Fe(CN)_6]_2$, $A_{0.4}M_{1.3}[Fe(CN)_6]$, and $AM[Fe(CN)_6]$. The A^+ cations are located in the cell interstitial sites, the cyanide groups, between M and Fe, have been largely omitted in this representation for the sake of clarity.*

Solid State Chemistry and Electrochemistry of Metal Hexacyanoferrates

Metal hexacyanoferrates have a face-centered cubic lattice (unit cell length: ~ 10.2 Å) with octahedral co-ordination of the M and Fe ions by -N≡C and -C≡N ligands respectively (10,11). The alkali metal cations, A (which provide charge compensation) are located in the tetrahedral sites (12) in these structures which may also contain co-

ordinated water molecules and anions in some cases. Representative structures and the corresponding compound stoichiometries are contained in Figure 1 for M and Fe in the +2 and +3 oxidation states respectively. Table 1 provides a listing of the electrochemically relevant compounds along with the corresponding M:Fe stoichiometries and formal oxidation states of the M and Fe sites for the six metals considered in this article.

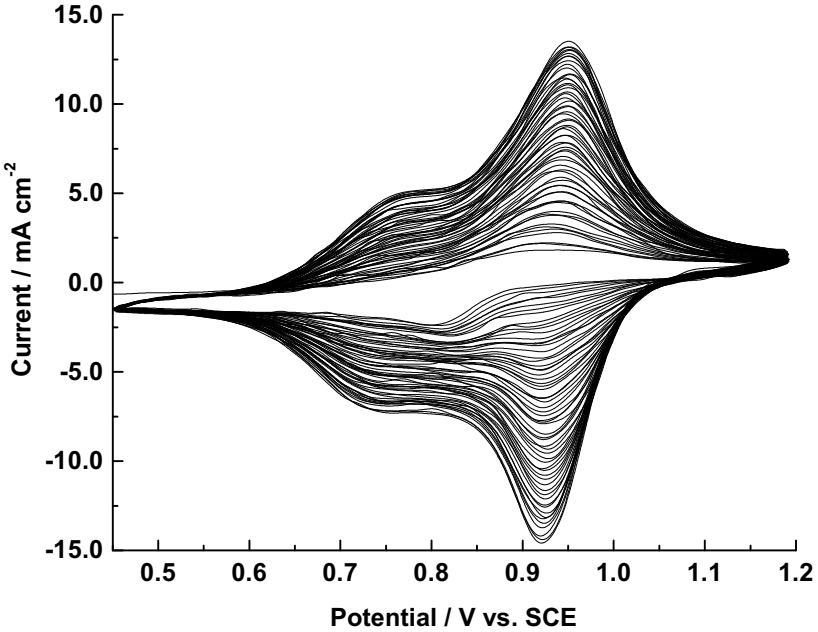

***Figure 2**: Cyclic voltammograms recorded during the growth of VHCF films on platinum substrates. The electrolytic solution consisted of: 1x10^{-3} M K_3 [Fe(CN)$_6$] + 1x10^{-3} M $NaVO_3$ in 3.6 M H_2SO_4 + 0.2 M K_2SO_4. The platinum electrode was kept polarized at 1.2 V in 3.6 M H_2SO_4 + 0.2 M K_2SO_4 during the addition of the film precursors in order to avoid incipient chemical coagulation of VHCF on the electrode surface. 50 potentiodynamic growth cycles at 100 mV s^{-1}.*

A change on the M oxidation state from +2 to +3 brings about a contraction of the M octahedral co-ordination manifold. This in turn manifests as a decrease in the unit cell dimension, a trend particularly well exemplified by the CoHCF compound system. In contrast, the octahedral co-ordination geometry is not significantly perturbed in size by the Fe oxidation state as borne out by the similarity between the unit cell parameters of $K_4[Fe(CN)_6]$ and $K_3[Fe(CN)_6]$ respectively (4).

In the case of the vanadium analog, X-ray photoelectron spectroscopy (XPS) and IR evidence (13,14) support the presence of VO^{2+} (vanadyl) ions in the compound structure. This would imply an octahedral coordination environment for the vanadium metal sites in which one of the six bridging CN ligands is replaced by a terminal oxygen. On the other hand, the measured V:Fe ratio of 1.5 ± 0.03 (14) suggests a trend in the

vanadium system that is common with the Cu, Pd, In, Co, and Ni analogs (Figure 1 and Table 1). Contrasting with an earlier study (13), evidence has been presented (14) for redox transitions in this compound to involve only the Fe sites, leaving the VO^{2+} sites intact. There are exceptions to this trend as noted later in this article. The simplified notation, VHCF, is used below with the implication that the vanadium metal cation is not present in the "free" state.

Mixed metal hexacyanoferrates have been prepared both as thin films and bulk precipitates (powders) as exemplified by the following compound: $K_{1.74-2y}Pd_y^{II}Ni_{1.13}^{II}[Fe^{II}(CN)_6]$ (where $y < 0.72$) (15). Rather than simple incorporation of Pd^{2+} at interstitial lattice positions, it has been hypothesized that at higher Pd^{2+} levels in solutions, palladium ions occupy nominally Ni positions in a -N≡C coordinated environment (15). Similar Ni/Co hybrid hexacyanoferrate networks have also been described (16).

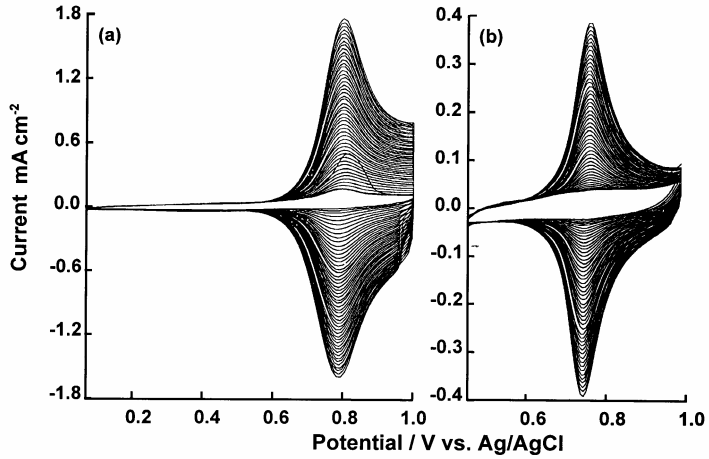

***Figure 3**: Cyclic voltammograms recorded during the growth of an InHCF film on a gold substrate using an extended (a) and a restricted potential window (b). Solution composition: 5 x 10^{-4} M $K_3[Fe(CN)_6]$ + 2.5 x 10^{-4} M $In_2(SO_4)_3$ in 0.5 M K_2SO_4 of pH 2. 50 potentiodynamic growth cycles at 50 mV s^{-1}.*

By tuning the oxidation state of the iron sites, it has been shown that the Ni or the In analogs behave either as redox-conducting solid electrolytes or as semiconductor/insulator materials (17). Thus the fully oxidized or fully reduced form of the Ni analog shows the voltammetric profile of an insulator. On the other hand, the mixed valence form containing both Fe^{II} and Fe^{III} redox sites shows semiconductor behavior. These data underline that the interplay between electron and ion fluxes depends on the openness of the structural network to ion motion and to factors such as hydration. Indeed electron diffusion in wet and dry Prussian blue films has been interrogated on interdigitated array electrodes (18). Other evidence from DC conductivity measurements shows a predominantly site-wise electron-hopping mechanism in truly dry Prussian blue and substituted metal analogs (19). Uptake of water provokes ionic conductivity in the system, and to the extent that electron hoping is coupled with ion motion to preserve

local charge neutrality, hydration of the material becomes an important factor in its overall charge transport behavior (17,20).

Other aspects of the solid-state chemistry of metal hexacyanoferrates (including that of the parent, Prussian blue) have been discussed by previous authors (1-8, 10, 11, 21).

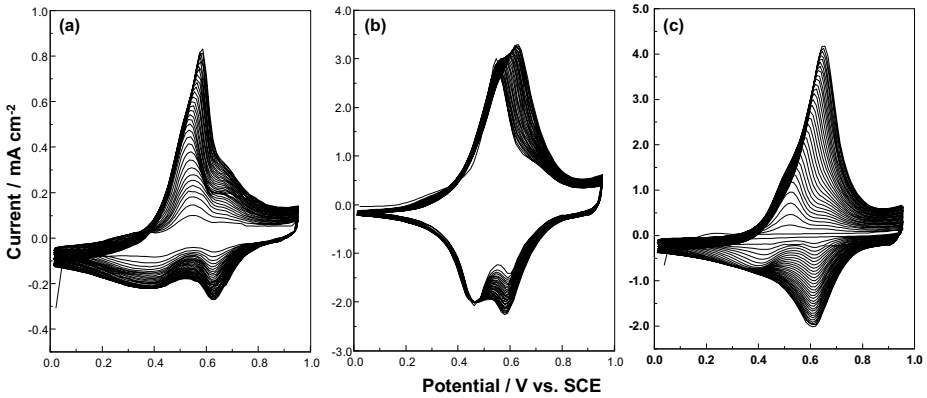

Figure 4*: Cyclic voltammograms recorded during the growth of CoHCF films on gold substrates using 1x10^{-3} $MK_3[Fe(CN)_6]$ + 1x10^{-3} $MCo(NO_3)_2$ mixed in deoxygenated 1 M KNO_3. 30 potentiodynamic growth cycles at 50 mV s^{-1}. (a) electrochemical thin film (δ = 80 nm) on non-protected gold, (b) chemical thick film (δ = 320 nm) (20 min at open circuit in precursor solution), (c) electrochemical thick film (δ = 335 nm) on electrochemically protected gold.*

Electrodeposition

Prussian blue itself has been prepared by both chemical (22,23) and electrochemical (24,25) methods. Here we will confine our discussion mostly to supported films of the metal hexacyanoferrate (MHCF) compounds. The most common strategy for electrosynthesis involves potentiodynamic cycling between pre-set potential limits of the working electrode in a supporting electrolyte containing both the metal ion (M^{n+}) and ferricyanide species. The metal ion can be dosed in situ into the growth medium from an active metal anode. This method has been used for the growth of the copper (26) and nickel (27-29) analogs. In other instances inert substrates such as glassy carbon, graphite, platinum, or gold are used. In these cases, the metal ions are added to the ferricyanide-loaded supporting electrolyte. Potentiodynamic cycling then instigates in situ precipitation of the (insoluble) MHCF compound on the inert film substrate surface. For applications wherein optical transparency of the entire film assembly is desired, conducting transparent oxide supports such as tin-doped indium oxide or F-doped SnO_2 glass may be used.

Figure 2 contains representative cyclic voltammograms signaling the growth of a VHCF film on a Pt substrate. Other than voltammetry, electrochemical quartz crystal microgravimetry (EQCM) (30,31) affords a sensitive probe of the mechanistic details associated with MHCF film growth. Such measurements have been described, for example, for InHCF (32) and NiHCF (33) during film growth. Elemental analysis via

atomic spectroscopy and XPS provides confirmation of the identity of the specific compound that has been deposited. The M:Fe atom ratio is a useful parameter in this regard (Table 1) as has been shown, for example, for the In, (34) V, (14) Co, (35) and Ni (36) analogs. Mössbauer studies have been reported (37) for CoHCF wherein the $Fe^{II/III}$ mixed-valent state was induced by ozonation. A very broad new line for the mixed-valent state was detected (37).

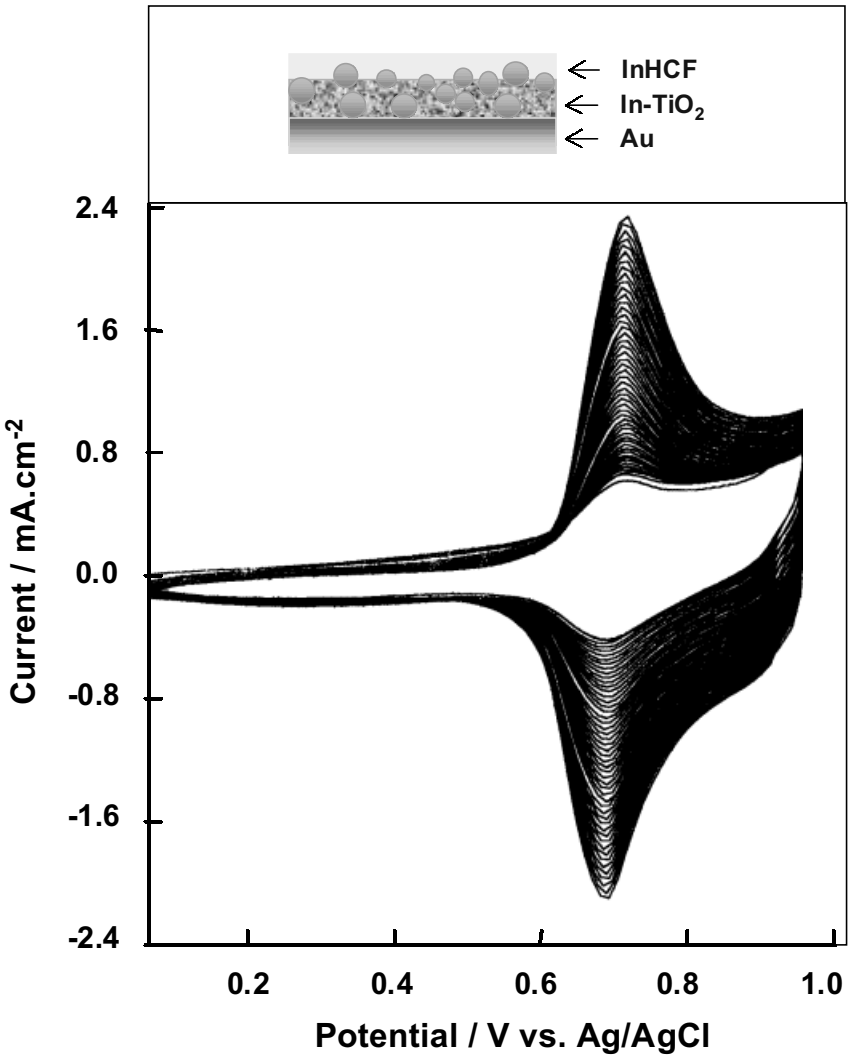

***Figure 5**: In-TiO_2 composite film grown on a gold substrate. Growth of a top layer of InHCF by repetitive cycling in a solution containing 5 x 10^{-4} M $K_3[Fe(CN)_6]$ and 2.5 x 10^{-4} M $In_2(SO_4)_3$ in 0.5 M K_2SO_4 (pH 4.5). 30 potentiodynamic growth cycles at 50mVs^{-1}. A schematic illustration of the In-TiO_2 composite film derivatized with InHCF is shown on top of this figure.*

The potential window deployed for potentiodynamic growth of the MHCF films can exert an influence on compound stoichiometry as exemplified by the InHCF system (38). Broader growth cyclic voltammetry profiles were discerned under "extended

potential window" (EPW) conditions relative to the "restricted potential window" (RPW) case (38). This is shown in Figure 3. The EPW film also grew at a faster rate compared to its RPW counterpart; compare the ordinate current scales in the two cases in Figure 3. These differences were rationalized on the basis that apart from the 1:1 (In:Fe) compound stoichiometry (Table 1), the 4:3 compound is also formed under the EPW condition (38).

Another striking example of the sensitivity of film morphology to the growth history is provided by the cyclic voltammetry data in Figure 4 for the CoHCF system (35). The three cases shown differ in the adjustment of the initial coagulation period prior to the electrosynthesis step and the extent of passivation of the gold substrate. Note that in the last case (Figure 4c) there is virtually no in situ precipitation when the potentiodynamic growth cycle is initiated. With a 20 minutes coagulation period (Figure 4b), the voltammetry profile is diagnostic of substantial CoHCF formation already when the potentiodynamic growth cycle is initiated (Figure 4b). The film morphology is roughest in this case.

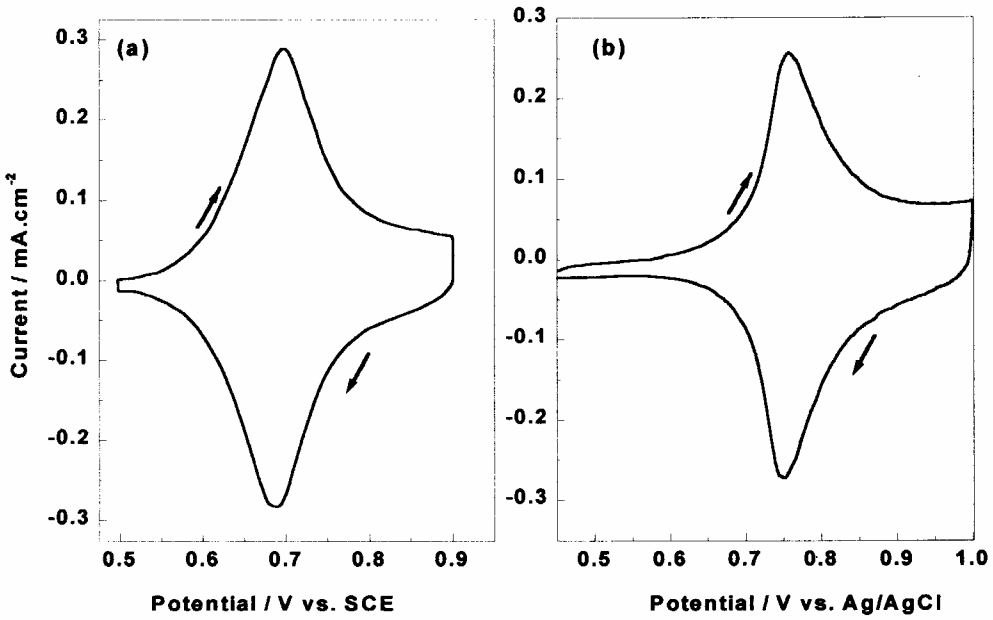

***Figure 6**: Cyclic voltammograms for a CuHCF film in contact with 0.5 M K_2SO_4 at a scan rate of 3.2 mV s^{-1} (a) and a InHCF film in 0.5 M K_2SO_4 (pH 2) at 5 mV s^{-1} (b).*

A method that is potentially applicable to prepare multilayers of MHCFs with different metal analogs, has been described (39). Self-assembly of mercaptopropionic acid was followed by subsequent attachment of CuHCF to the thiol and carboxylate functionalities of the template layer (39). Multiple sequential adsorption of metal ions and hexacyanometalate anions was also used to deposit several MHCF analogs on solid supports with monolayer precision (40,41). Other studies oriented toward the preparation of Langmuir-Blodgett films of Prussian blue are exemplified by Ref. 42. Highly-ordered Prussian blue nanowire arrays (nanowire diameter: ~50 nm, length: up to 4 μm) were fabricated (43) using electrodeposition in an alumina (alumite) template (44). Finally,

CuHCF (and other magnetic compounds) were prepared on the nanometer size scale by controlled co-precipitation involving mixtures of water-in-oil microemulsions (45).

Metal hexacyanoferrate compounds can also be mated with semiconductor particles (46). In the electrosynthetic approach, the growth medium is simply dosed with the semiconductor particles to the desired level (usually in the range of several mg/L). Alternately, a single crystal semiconductor surface can be coated with MHCF via electrodeposition as demonstrated for n-TiO_2 (47) and n-$SrTiO_3$ (48). A variant of this approach involves the use of polycrystalline semiconductor films on which the MHCF layer is subsequently coated (49-51). Finally, metal/semiconductor (M/S) composite coatings can be subsequently derivatized by exposing them to ferricyanide (52-54). The M component in the composite is converted in situ to the corresponding MHCF layer (see above) in this manner, Figure 5. The reader is also referred to other studies (13,14, 55-60) for further details of MHCF film growth by electrochemical methods.

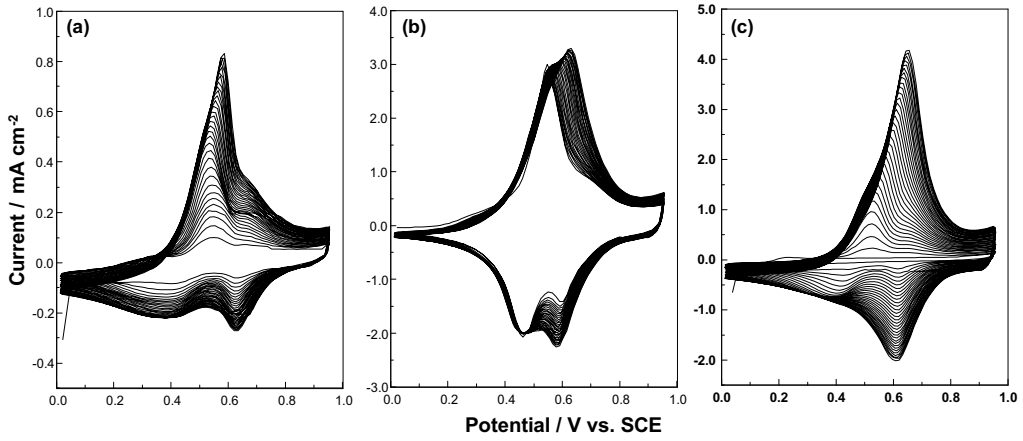

Scheme I

Redox Transformations and Ion Fluxes

Once the MHCF layer is grown on a targeted surface, the chemically modified electrode assembly can be transferred to a medium containing only the supporting electrolyte. Subsequent cyclic voltammetry reveals one or more reversible waves signaling redox processes of the MHCF layer. The complexity of this voltammogram depends on the particular system, and how many compound stoichiometries (Table 1) are inherent in the deposited layer. Particularly clean profiles are seen for the Cu and In

analogs (the latter under a restricted potential window growth condition, see above) as shown in Figures 6a and b respectively. Note that the voltammetry waves in this figure are sharp, symmetrical and with no diffusion tails in either positive- or negative- going cycles. Further, peak potential separation is close to zero in both cases. These trends are diagnostic of surface-confined location of the MHCF redox process (61,62).

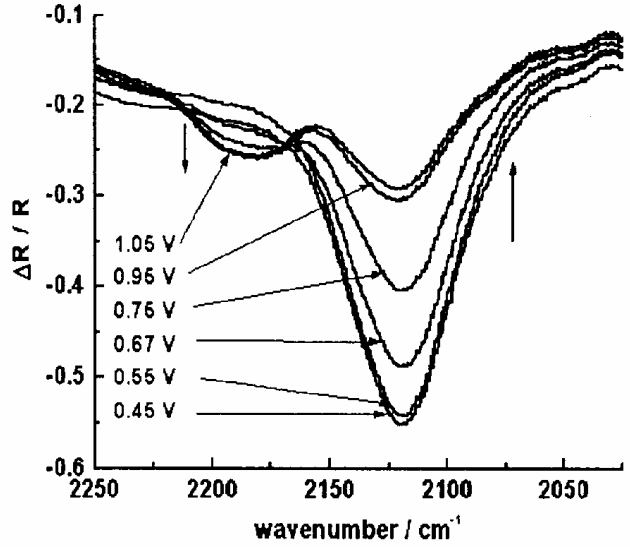

***Figure** 7: In situ infrared reflectance spectra of CuHCF in 0.5 M K_2 SO_4. The spectra were obtained at stepwise increasing potentials from 0.45 V up to 1.05 V as indicated in the figure. Arrows indicate the evolution of the respective bands. The reference spectrum is that of a bare gold electrode.*

Pertinent here is the influence of counter-ion motion on the voltammogram profiles. Recall that alkali cation flux into and out of the MHCF layer is critical to maintaining local charge neutrality during film redox (62). Even early studies (63,64) on this topic revealed the sensitivity of the voltammetry profiles to electrolyte cations. For example, the introduction of Cs^+ caused multiple wave formation in the NiHCF system; interestingly, changing the supporting cation from one to another and then back to the first, reproduced the original cyclic voltammogram (63). The redox reaction in CuHCF was seen to be faster in a medium having ammonium ion than in a K^+-containing electrolytes (64). Nernstian semi-log plots of peak potentials versus ammonium ion concentration were also presented in this early study (64). Similar data exist for K^+, NH_4^+ or Na^+ ions in the CuHCF and CoHCF systems (65-67).

Loss of electroactivity has been observed for Rb^+ and Cs^+-containing electrolytes when CoHCF films are voltammetrically cycled (60,68). These changes in electroactivity were attributed to the rather large hydrated radii of Rb^+ and Cs^+ ions and inhibition of their ingress/egress into/out of the MHCF framework. Similar voltammetric "passivation" of the CoHCF film in Li^+ containing electrolytes has been attributed to the large hydration sphere of Li^+ cations (60). The formal potentials of CoHCF films were measured for Li^+, Na^+, K^+, and Cs^+ containing electrolytes, and were found to correlate well with the sizes of the hydrated ions (69). Ion permeability in an InHCF film was

reported to follow the order: $Na^+ > K^+ > NH_4^+ > Li^+$ in two separate studies (70,71). Cyclic voltammograms were presented for NiHCF films in 13 different cation-containing supporting electrolytes (60). Other voltammetric studies pertaining to the effect of electrolyte cations include Ref. 72 on CoHCF.

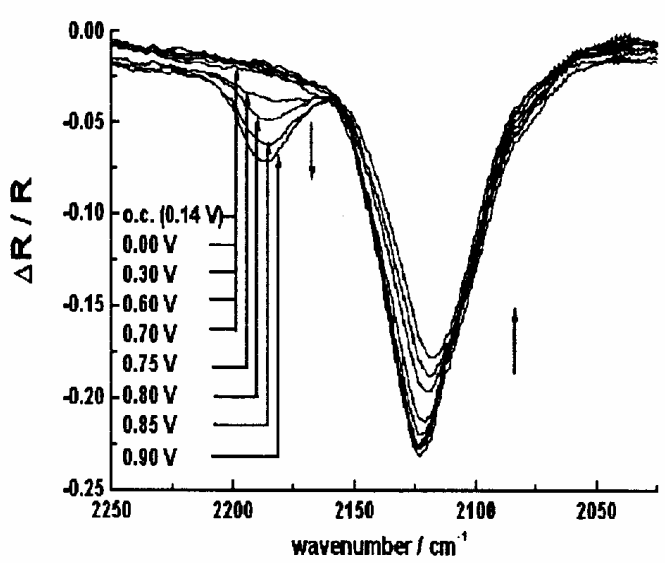

***Figure 8**: In situ infrared reflectance spectra of an InHCF film electrodeposited on gold using EPW conditions. The spectra were obtained in 0.5 M K_2SO_4 at pH 2. Applied potentials as indicated in the figure.*

The EQCM technique affords another sensitive in situ probe of the ion fluxes during MHCF film redox. This is exemplified by measurements on InHCF (67), CoHCF (59,69) and NiHCF (59,73). Beam deflection techniques were also employed for monitoring ion transport during redox reactions of InHCF surface layers (74). The principal charge compensating ions were shown (74) to be cations (however see below). X-ray absorption near-edge structure (XANES) experiments indicate the chemical environment of Co(II) sites to be influenced by the presence of hydrated alkali metal counter-ions (69). Finally, oxidation state profiles in NiHCF derivatized electrodes were mapped with the use of line-imaging Raman spectroscopy (75).

While alkali cations are the principal charge-compensating species in redox reactions of MHCF films, radiotracer evidence on InHCF points toward contributions from anion fluxes as well (67). This manifests mainly for the M:Fe 4:3 compound stoichiometry (see also Table 1). Anion fluxes are also shown both by survey XPS scans and quantitative assays for S (arising from sulfate anions) in the InHCF system (38). Similar behavior appears to hold in the vanadium case (14). Interestingly, the probe beam deflection technique indicated a contribution of anion fluxes in InHCF of only less than 7%, at least for film potentials below 0.9 V (versus saturated calomel electrode reference) (74). The double injection of electrons and cations was also studied by monitoring time-resolved changes in the optical reflectivity of Prussian blue-modified Pt disk electrodes during galvanostatic reduction of the film (76).

Spectroelectrochemistry

Spectroelectrochemistry combines two powerful techniques, namely spectroscopy and electrochemistry, for studying the changes occurring during redox of the test system (77-81). Thus, oxidation states can be changed electrochemically by addition or removal of electrons at an electrode while spectral measurements, at the electrode surface or in the solution adjacent to the electrode, are made simultaneously. Importantly, this combined approach obviates a key shortcoming of electrochemical probes associated with their chemical non-specificity (82). In this section, the application of IR and UV-visible spectroelectrochemical probes to the MHCF system will be discussed.

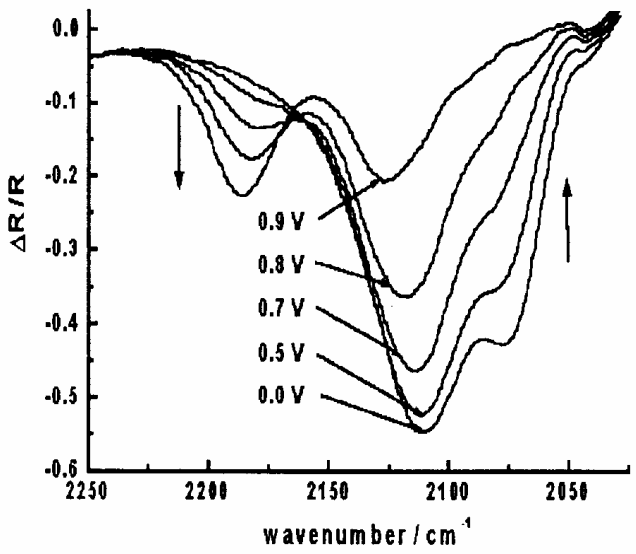

Figure 9*: In situ infrared reflectance spectra of a PdHCF film in 1 M KCl (pH 2.5) at stepwise increasing potentials (as indicated in the figure). Applied potentials as shown in the figure. The reference spectrum was taken on a bare platinum electrode.*

The cyanide group-stretching region in the IR spectrum (spanning ca. 2000 – 2250 cm^{-1}) provides a sensitive and versatile probe for compounds in the MHCF family (21, 29, 83-85). Diffuse reflectance Fourier transform (FT) IR data, *ex situ*, were presented for NiHCF in an early study (29), where the virtues associated with spectra acquired *in situ* in an electrochemical cell (i.e., in a spectroelectrochemical experiment), were pointed out by these authors. Subsequent studies have examined the *in situ* FTIR behavior of other compounds, e.g., CoHCF (86).

We will now present more recent examples drawn from our own studies on a set of MHCF compounds. Scheme I provides a compilation of the redox transformations with the corresponding compound compositions and related CN stretching signatures for the various members of the MHCF family. This scheme was synthesized from our own data obtained by cyclic voltammetry and infrared spectroelectrochemistry of the various MHCF compounds.

A brief description of the IR spectrolectrochemistry of Cu, In, Pd, Co and V analogs is described next. Thus, Figures 7 through 11 were obtained in the external reflectance mode, the output being examined as the normalized difference between the

signal at a given potential and that from the bare electrode, no film, taken as reference, R_{ref}, i.e. $\Delta R/R_{ref} = (R - R_{ref})/R_{ref}$. Changes in the spectral bands, as the applied potential is sequentially changed, report on the redox conversion of the particular MHCF under studied. Further, the complexity of the in situ spectral profiles points toward the possibility of formation of multiple compounds in each system (see Table 1). While the profiles are particularly simple for CuHCF (Figure 7) and InHCF (Figure 8), increasing complexity then follows the order: PdHCF < CoHCF < VHCF (see Figures 7 to 11).

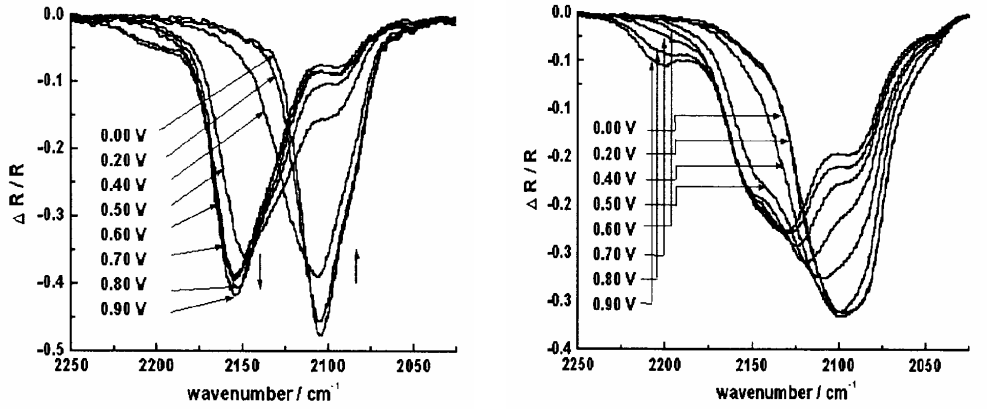

***Figure 10**: In situ infrared reflectance spectra of a CoHCF thin (surface loading, $\Gamma = 6 \times 10^{-8}$ mol/cm^2) (a) and thick film ($\Gamma = 2 \times 10^{-7}$ mol/cm^2) (b) respectively in M KNO_3. Applied potentials as indicated in the figure. The reference spectrum was taken on a bare gold electrode.*

Figure 7 shows the infrared spectral evolution as a function of potential for a thin CuHCF film (53 nm of thickness). Spectra were obtained at set potentials (0.45 V, 0.55 V, 0.67 V, 0.95 V and 1.05 V) showing that oxidized and reduced forms of CuHCF can coexist in the film. A single intense band at 2119 cm^{-1} was detected at the lower potential (0.45 V). This band is progressively being converted to a band at 2179 cm^{-1} corresponding to the oxidized state of the film. At 1.05 V, the spectrum is made of two bands, the 2179 cm^{-1} band that peaks at this higher potential and a small remaining band at 2119 cm^{-1}. For this system there is a highly reversible charge transfer process, although some non-active centers remain reduced at the highest potential used. Interestingly, a higher reversibility for conversion of species was observed for thicker films (in the range of 150 to 400 nm), as the non-active redox centers were relatively more prominent in thin CuHCF films (< 150 nm) (87). These CN characteristic frequencies can be assigned to a film stoichiometry with a Cu/Fe ratio of 3/2 as indicated in Scheme I.

In situ spectroelectrochemical data for InHCF films is shown in Figure 8 for progressively increasing potentials from 0.0 V to 0.90 V. The data correspond to a film grown under EPW conditions. These spectra are made up of two main bands located at 2130 cm^{-1} for the reduced centers and at 2187 cm^{-1} for the corresponding oxidized species. The amount of redox centers that reversibly convert is just ca. 25 % of the total number.However, this reversible portion of the film keeps itself highly active without

interference from the non-active reduced species that make up the main film component. The two bands at 2130 cm^{-1} and 2187 cm^{-1} correspond to a compound stoichiometry bearing a In/Fe ratio of unity (see Scheme I). Additionally, difference reflectance measurements (not shown) signaled the presence of two weak bands contributions peaking at 2100 and 2120 cm^{-1} that correspond to a redox conversion of InHCF species having a In/Fe ratio of 4/3. These are also included in Scheme I.

Figure 9 shows a set of spectra for a PdHCF film. The behavior of PdHCF has been reported elsewhere (88). Briefly the reduced state of the film is characterized by bands at 2075 and 2110 cm^{-1}, the fully oxidized state being represented by bands at 2130 and 2180 cm^{-1}. The interrelation of these two sets of bands, corresponding to the reduced and oxidized parent states of PdHCF, is best brought out either through difference spectra or dynamically by potential-modulation spectroscopy (88). Based on Figure 12 and other difference spectra data (not shown), we pair the 2075 cm^{-1} / 2180 cm^{-1} and the 2110 cm^{-1} / 2130 cm^{-1} infrared features as pertaining to redox partners, the first corresponding to a stoichiometry with a Pd/Fe ratio of unity and the second with a ratio of 3/2. Both are included in Scheme I.

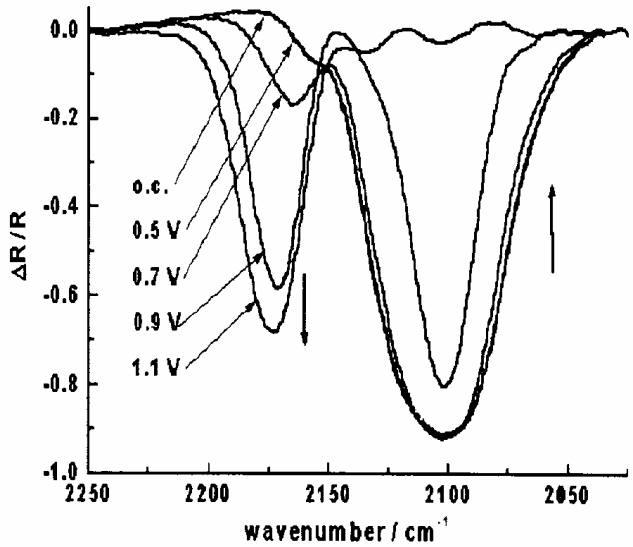

Figure 11*: In situ infrared reflectance spectra of a VHCF in 3.6 M H_2SO_4 + 0.2 M K_2SO_4 Applied potentials as indicated in the figure. The reference spectrum was taken on a bare platinum electrode.*

For the CoHCF system, Figure 10 shows two sets of spectra corresponding to a thin (6 x 10^{-8} mol/cm^2) and a thick film (2 x 10^{-7} mol/cm^2). For the thin film (Figure 10a) a band at 2105 cm^{-1} with a shoulder at 2087 cm^{-1} can be observed at 0.0 V. These two bands are progressively disappearing, as the potential is made more positive. At the higher potential set (0.9 V), two bands are seen at 2155 and 2200 cm^{-1}. There is also a small rest of the 2100 cm^{-1} band that points to the presence of some inactive reduced species in the film. A more complex spectral behavior was found for thick CoHCF films (Figure 10b). Here, for the 0.0 – 0.4 V potential range, there are two bands at 2087 and 2105 cm^{-1}. Then, a new spectral profile is observed as from 0.5 V made up of two main

features, a dominant band in the range of 2113 – 2130 cm^{-1} that shifts with potential and other less important band at 2155 cm^{-1} that increases in intensity as the potential is made more positive. Finally, when the potential reaches values of 0.8 V and beyond, a band at 2220 cm^{-1} starts making a neat contribution. Combining these spectral data with characterization by XPS (35), it is possible to make assignments of the different band signatures to the corresponding CoHCF compound stoichiometries, Scheme I.

Figure 11 shows a set of spectra for a VHCF film, which as in the case of CoHCF, is particularly complex with at least four participant species implicated in the redox process (see Scheme I). At potentials lower than 0.7 V the spectra are made of a quite broad band that can be deconvoluted in two components peaking at 2097 and 2103 cm^{-1}. At the higher potential used (1.1 V) the spectrum is made of three bands at 2103, 2135, and 2170 cm^{-1}. These CN signatures were assigned to two distinct film stoichiometries by using supplementary data from cyclic voltammetry and UV-Visible reflectance spectroscopy as included in Scheme I.

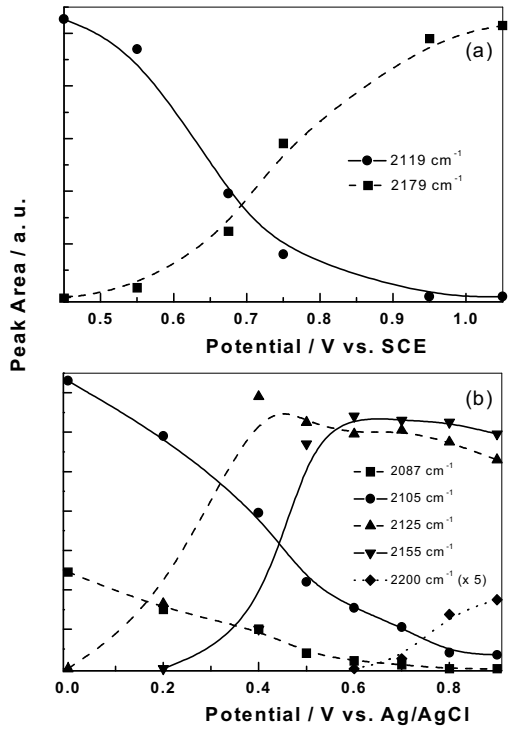

Figure 12*: Peak areas of deconvoluted infrared bands as a function of potential for CuHCF (Fig. 12a) and CoHCF (Fig. 12b) films. Areas were integrated over the spectra in Figures 7 and 10 respectively.*

The redox transformations undergone by the various participating species in each system (Table I) can be better discerned by plotting the peak area of the deconvoluted IR bands as a function of potential. Two examples of such plots are shown for CuHCF (Figure 12a) (87) and CoHCF (Figure 12b) (35). The differences in the complexity of the overall redox process are striking for the two cases. Finally, it must be pointed out that the spectral changes shown in Figures 7 to 12 as a function of potential are completely

reversible in that comparable data are obtained on reverting the potential back to the initial value.

Turning to spectroelectrochemistry with spectral changes monitored in the UV-visible region, data can be acquired in situ either in the transmission or in the reflectance mode. In an early study (89), diffuse reflectance UV-visible spectroelectrochemistry on NiHCF was shown to be both species specific and sensitive to the amount of surface-confined material and its oxidation state. Another useful approach involves acquisition of the UV-visible spectral data (at selected wavelengths) while the electrode potential is slowly scanned as in a voltammetry experiment (62, 88, 90). The resultant data, processed in the form of a time derivative signal versus electrode potential, bear a striking resemblance to cyclic voltammograms except for the important distinction that the scans are species-specific (62, 88, 90). Such data have been presented for CoHCF (91). UV-visible spectroelectrochemistry has also been utilized to determine the electron stoichiometry during redox of InHCF in aqueous electrolytes (70), according to methodology developed by other authors (92).

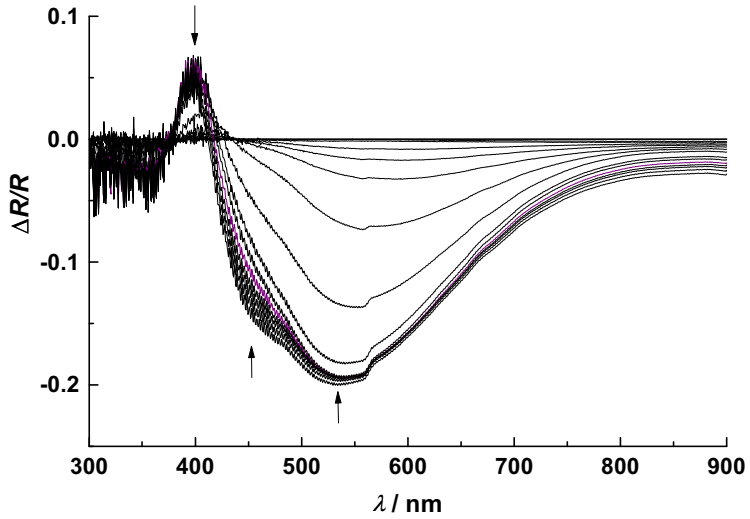

***Figure 13**: In situ UV-Vis reflectance spectra, $\Delta R/R = [(R-R_{0.05\ V}) /R_{0.05\ V}]$ for a CoHCF film in 1 M KNO_3. Spectra were collected every 0.02 V during a cyclic potential sweep at 5 mV s^{-1} in the 0.05 V - 0.95 V range. For the sake of clarity, only a selected sub-set of spectra are shown on a negative-going scan. Spectra, 20X averaged, were obtained at an incidence angle of 45° with an exposure time of 0.03 s. The spectrum of the film at 0.05 V was taken as reference. CoHCF loading: $\Gamma = 6 \times 10^{-8}$ mol cm^{-2}.*

UV-visible spectroelectrochemical studies on the MHCF system were performed on a custom-built optical multichannel analyzer fitted with a cooled Si diode array detector (88, 93-95). Reflectance spectra were acquired during slow (nominally 5 mV s^{-1}) linear potential scans of the MHCF-modified electrodes. Data are displayed as plots of ΔR/R versus wavelength. Unlike the IR experiments discussed earlier, intensities in the UV-visible experiments are normalized to that of a spectrum taken, in the presence of the film, at the lower limit of the potential window used. Other details may be found in Refs. 88, and 93 through 95.

Table 2 contains a compilation of peak wavelengths (λ_{max}), for the absorption of various MHCF compounds dealt with in this article in their oxidized and reduced states. The relevance of such data to the electrochromic applicability of these compounds can be inferred from the contrasting film coloration obtained at the reduced and oxidized states of the various MHCF films (Table 3). Here, the utility of UV-visible spectroelectrochemistry in studying the MHCF redox process (es) is considered. Taking into account that UV-visible spectroelectrochemical data are species-specific (see above and Ref. 89), the trends in Table 2 support our earlier ordering of the MHCF compounds (CuHCF < InHCF < PdHCF < CoHCF < VHCF) in terms of the complexity of the redox process.

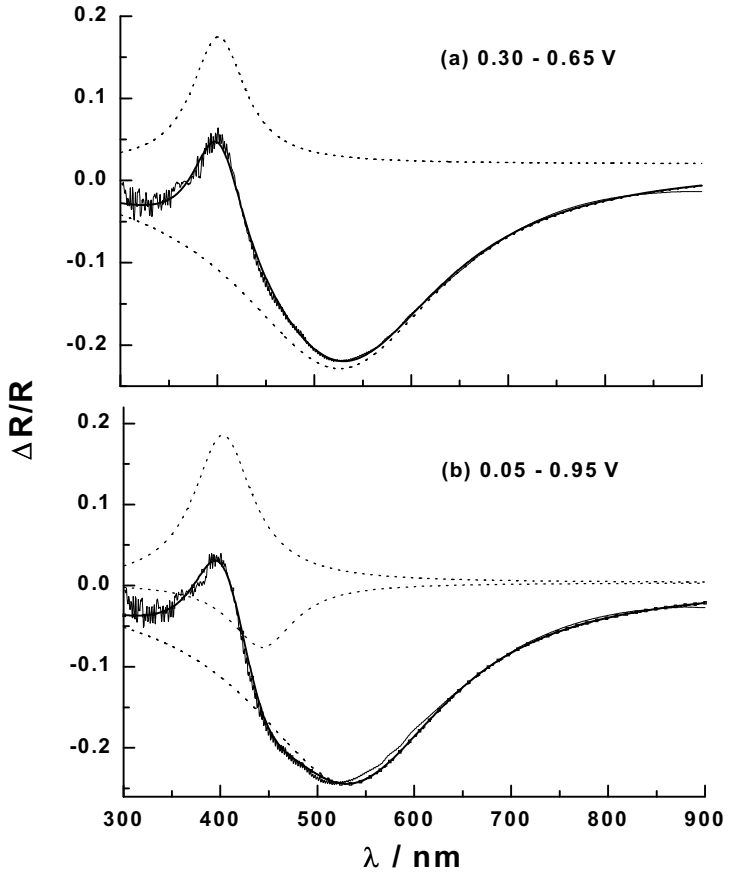

Figure 14*: Deconvolution of two UV-Vis difference ΔR/R spectra obtained in the potential range: 0.30 – 0.65 V (Fig. 14a) and 0.05 – 0.95 V (Fig.14b) for CoHCF.*

We focus our attention now on the two more complex systems, namely CoHCF and VHCF, starting with Figures 13-15 that contain data for CoHCF. The overlaps in the spectra for the oxidized and reduced states of CoHCF (91) manifest in terms of the bipolar character of the ΔR/R vs. λ profiles in Figure 13 (see also Figure 3 in Ref. 91). Three main signatures at 380 nm, 440, and 530 nm (Table 2) are clearly seen in the spectral evolution in Figure 13, especially in the deconvoluted spectra in Figure 14. The change with potential of the three bands is further expanded in Figure 15. Interestingly,

the two arrests in the 380 nm profile (at ~0.50 V and 0.67 V in the positive-going scan and at 0.26 and 0.40 in the negative-going sweep) suggest a 380/440 nm and 380/530 nm pairing of the probes for the two main redox centers.

***Table 1**: Compound Stoichiometries and Metal Oxidation States in Prussian Blue (MHCF) Analogs. [a)] The oxidation state, in the case of vanadium, refers to oxygen-bonded species rather than the "free" metal cation; see text.*

metal	Formula	M:Fe ratio	M, Fe Formal oxidation state[a)]
copper	$K_2Cu_3[Fe(CN)_6]_2$	3:2	II, II
	$Cu_3[Fe(CN)_6]_2$	3:2	II, III
Palladium	$K_2Pd_3[Fe(CN)_6]_2$	3:2	II, II
	$Pd_3[Fe(CN)_6]_2$	3:2	II, III
	$K_2Pd[Fe(CN)_6]$	1:1	II, II
	$KPd[Fe(CN)_6]$	1:1	II, III
Indium	$In_4[Fe(CN)_6]_3$	4:3	III, II
	$KIn_4[Fe(CN)_6]_3(SO_4)_2$	4:3	III, III
	$KIn[Fe(CN)_6]$	1:1	III, II
	$In[Fe(CN)_6]$	1:1	III, III
Vanadium	$K_2\ (VO)_3\ [Fe(CN)_6]_2$	3:2	II, II
	$(VO)_3\ [Fe(CN)_6]_2$	3:2	II, III
	$K_3(VO_2)_3\ [Fe(CN)_6]_2$	3:2	I, III
	$K_{1.4}\ (VO)_{1.3}\ [Fe(CN)_6]$	4:3	II, II
	$K_{0.4}\ (VO)_{1.3}\ [Fe(CN)_6]$	4:3	II, III
cobalt	$K_2Co_3[Fe(CN)_6]_2$	3:2	II, II
	$Co_3[Fe(CN)_6]_2$	3:2	II, III
	$K_{1.4}Co_{1.3}[Fe(CN)_6]$	4:3	II, II
	$K_{0.4}Co_{1.3}[Fe(CN)_6]$	4:3	II, III
	$K_2Co[Fe(CN)_6]$	1:1	II, II
	$KCo[Fe(CN)_6]$	1:1	II, III
	$Co[Fe(CN)_6]$	1:1	III, III
nickel	$K_2Ni_3[Fe(CN)_6]_2$	3:2	II, II
	$Ni_3[Fe(CN)_6]_2$	3:2	II, III
	$K_2Ni[Fe(CN)_6]$	1:1	II, II
	$KNi[Fe(CN)_6]$	1:1	II, III

***Table 2**: Wavelength Maxima for the Oxidized and Reduced Redox States of MHCF Compounds.* [a] *From Ref. 89.*

Compound	λ_{max}, nm	
	oxidized state(s)	reduced state(s)
CuHCF	405	495
InHCF	495	360
PdHCF	440	425
CoHCF	440, 530	380
NiHCF[a)]	405	320
VHCF	515, 600, 780	390, 455

***Table 3**: Electrochromic Color Changes in the Various MHCF Compounds*[a)]*.* [a] *Also see Ref. 71.* [b] *Color shown to depend on various factors; refer to text and Ref. 60*

Compound	Color	
	reduced state	oxidized state
CuHCF	red-brown	Yellow
InHCF	White	Yellow
PdHCF	Green	Orange
CoHCF[b)]	Green	Violet / magenta
NiHCF	Grey	Yellow
VHCF	Yellow	blue-green

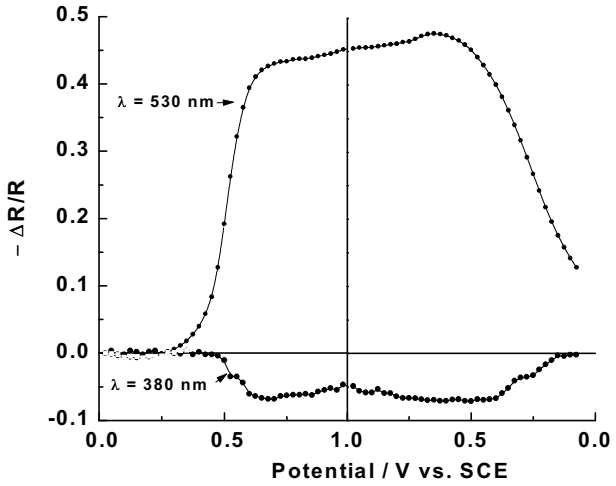

***Figure 15**: Evolution of the main bands peaking at 380 nm (reduced species), 440 nm (oxidized species), and 510 nm (oxidized species) for CoHCF as a function of electrode potential. Data obtained from spectra in Figure 13.*

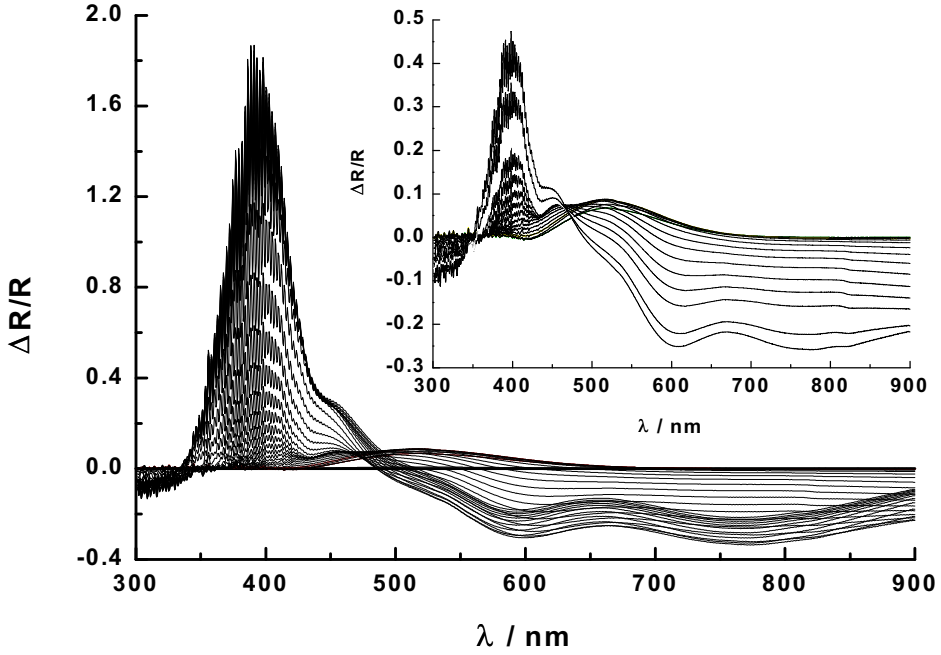

***Figure 16**: In situ UV-Vis reflectance spectra, ΔR/R = [(R-$R_{0.45\ V}$) /$R_{0.45\ V}$] for a VHCF film in 3.6 M H_2SO_4 + 0.2 M K_2SO_4. Spectra were collected every 0.025 V during a cyclic potential sweep at 5 mV s^{-1} in the 0.40 V – 1.20 V range. For the sake of clarity, the insert contains only the spectra obtained in to the 0.40 V – 0.95 V range. All spectra are referred to the spectrum at 0.45 V. VHCF loading: 3.2 x 10^{-7} mol/cm^2. Other details as in Figure 13.*

We tentatively assign the 380 nm signature to the Fe(II), Co(II) redox pairs, and the 440 nm and 530 nm signatures to the Fe(III), Co(II) and Fe(II), Co(III) counterparts respectively. The possibility for the 440 nm signature to have a contribution from the Fe(III), Co(III) pair (Scheme I) has been discarded by noting that the intensity of the 530 nm band does not decrease when the 440 nm signature increases (Figure 15). A band at approximately this wavelength has been assigned to a d-d transition involving high-spin Co(II) sites (96). A further discussion of the UV-visible band assignments may be found in Refs. 69, 96 and 97.

Figures 16 and 17 show relevant UV-visible spectroelectrochemical data for the VHCF system. The observation of at least five spectral signatures in this case belies the *apparent* simplicity of the voltammogram profiles for this system that shows only two (albeit broad) sets of waves (68) (Figure 2; see also Ref. 14). The bands at 600 nm and 780 nm may be assigned to the vanadyl (VO^{2+}) species that appear implicated in the first voltammetric peak (more negative potentials) while the second peak is likely associated with the electrooxidation of vanadyl to vanadate (VO_2^+) species. The VO_2^+ species do not absorb in the UV-visible spectral region (98). The evolution with potential of three selected bands for VHCF is presented in Figure 17. When compared with its counterpart in Figure 15 for CoHCF, the vanadium system appears to be considerably more complex. Further work on VHCF is needed to unravel the *chemical* details of its redox processes.

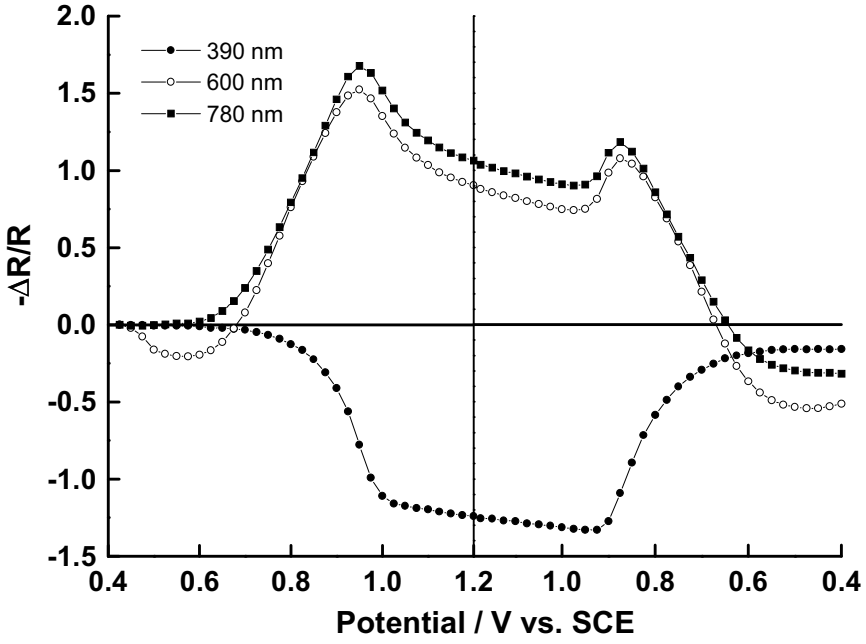

Figure 17*: Evolution of the main bands peaking at 390 nm (reduced species), 600 nm (oxidized species), and 780 nm (oxidized species) as a function of electrode potential for VHCF. Data obtained from the spectra in Figure 16.*

Concluding Remarks

This article has hopefully served to underline the enormous range and scope in the chemical composition, properties, and spectroelectrochemical signatures of Prussian blue analogs. Six such compounds were considered in this article. While the earlier studies focused on Prussian blue itself, other transition metal hexacyanoferrates (and hexacyanometalates in general) are beginning to attract attention from chemists, physicists, and material scientists alike. In the crystal ball of the authors, this trend is expected to continue well into the future. It is our hope that this article will spur the interest of new researchers in these interesting compounds, and in a small way, will contribute to the continued vitality of this field.

Acknowledgments

This research was funded in part by grants from the Argentine Science Research Council, CONICET, and the U.S. Department of Energy, Office of Basic Energy Sciences. Exchange of visits between the two participant institutions, was facilitated by travel grants from CONICET and the National Science Foundation (U.S.-Argentina International Programs).

References

(1) Itaya, K.; Uchida, I.; Neff, V. D. *Acc. Chem. Res.* **1986**, *19*, 162. See also references therein.

(2) Monk, P. M. S.; Mortimer, R.J.; Rosseinsky, D. R. *Electrochromism: Fundamentals and Applications,* VCH: Weinheim, **1995**. See also references therein.
(3) Brown, D. B. *Mixed-Valence Compounds: Theory and Applications in Chemistry, Physics, Geology and Biology,* NATO Advanced Study Institute Series, D. Reidel: Doredrecht, The Netherlands, **1980**.
(4) Sharpe, A. G. *The Chemistry of Cyano Complexes of the Transition Metals,* Academic Press: New York, **1976**.
(5) Chadwick, B. M.; Sharpe, A. G. *Adv. Inorg. Chem. Radiochem.* **1966**, *8*, 83.
(6) Robin, M. B.; Day, P. *Adv. Inorg. Chem. Radiochem.* **1967**, *10*, 247.
(7) Keggin, J. F.; Miles, F. D. *Nature (London)* **1936**, *137*, 577.
(8) Buser, H. J.; Schwarzenbach, D.; Petter, W.; Ludi, A. *Inorg. Chem.* **1977**, *16,* 2704.
(9) *The Electrochemical Society Interface,* Special Issue on Molecular Magnets, Fall **2002**, *11* (3).
(10) Ludi, A.; Gudel, H. U. in *Structure and Bonding;* Dunitz, J. D., Ed., Springer-Verlag: Berlin, **1973**; Vol. 14, pp. 1-21.
(11) Herren, F.; Fischer, P.; Ludi, A.; Hälg, W. *Inorg. Chem.* **1980**, *19*, 956.
(12) West, A. R. *Basic Solid State Chemistry,* Wiley: Chichester, 1999; Chap. 1, p. 25.
(13) Shaojun, D.; Fengbin, Li, *J. Electroanal. Chem.* **1986**, *210*, 31.
(14) Carpenter, M. K.; Conell, R. S.; Simko, S. J. *Inorg. Chem.***1990**, *29*, 845.
(15) Kulesza, P. J.; Malik, M. A.; Schmidt, R.; Smolinska, A.; Miecznikowski, K.; Zamponi, S.; Czerwinski, A.; Berrettoni, M.; Marassi, R. *J. Electroanal. Chem.* **2000**, *487*, 57.
(16) Kulesza, P. J.; Malik, M. A.; Skorek, J.; Smolinska, A.; Miecznikowski, K.; Zamponi, S.; Berrettoni, M.; Giorgetti, M.; Marassi, R. *J. Electroanal. Chem.* **1999**, *146*, 3757.
(17) Kulesza, P. J. *Inorg. Chem.* **1990**, *29*, 2395.
(18) Feldman, B. J.; Murray, R. W. *Inorg. Chem.* **1987**, *26*, 1702.
(19) Rosseinsky, D. R.; Tonge, J. S.; Berthold, J.; Cassidy, J. F. *J. Chem. Soc.; Faraday Trans.* **1987**, *83*, 231.
(20) Xidis, A.; Neff, V. D. *J. Electrochem. Soc.* **1991**, *138*, 3637.
(21) Ayers, J. B.; Waggoner, W. H. *J. Inorg. Nucl. Chem.* **1971**, *33*, 721.
(22) Neff, V. D. *J. Electrochem. Soc.* **1978**, *125*, 886.
(23) Ellis, D.; Eckhoff, M.; Neff, V. D. *J. Phys. Chem.* **1981**, *85*, 1225.
(24) Itaya, K.; Akahoshi, H.; Toshima, S. *J. Electrochem. Soc.* **1982**, *129*, 1498.
(25) Kellawi, H.; Rosseinsky, D. R.; *J. Electroanal. Chem.* **1982**, *131*, 373.
(26) Siperko L. M.; Kuwana, T. *J. Electrochem. Soc.* **1983**, *130*, 396.
(27) Bocarsly, A. B.; Sinha, S. *J. Electroanal. Chem.* **1982**, *137*, 157.
(28) Sinha, S.; Humphrey, B. D.; Fu, E.; Bocarsly, A. B. *J. Electroanal. Chem.* **1984**, *162*, 351.
(29) Sinha, S.; Humphrey, B. D.; Bocarsly, A. B. *Inorg. Chem.* **1984,** *23*, 203.
(30) Schumacher, R. *Angew. Chem. Int. Ed. Engl.* **1990**, *29*, 329.
(31) Buttry, D. A.; Ward, M. D. *Chem. Rev.* **1992**, *92*, 1355.
(32) Czirok, E.; Bácskai, J.; Kulesza, P. J.; Inzelt, G.; Wolkiewicz, A.; Mielcznikowski, K.; Malik, M.A. *J. Electroanal. Chem.* **1996**, *405*, 205.

(33) Bácskai, J.; Martinvoz, K.; Czirok, E.; Inzelt, G.; Kulesza, P. J.; Malik, M. A. *J. Electroanal. Chem.* **1995**, 385, 241.
(34) Cataldi, T. R. I.; de Benedetto, G. E.; Bianchini, A. *J. Electroanal. Chem.* **1998**, *448,* 111.
(35) Lezna, R. O. ; Romagnoli, R.; de Tacconi, N. R.; Rajeshwar, K. *J. Phys. Chem. B* 2002, *106*, 3612.
(36) Cataldi, T. R. I.; Guascito, R. ; Salvi, A. M. *J. Electroanal. Chem.* **1996**, *417*, 83.
(37) Reguera, E.; Bertran, J. F.; Diaz, C.; Blanco, J. ; Rondon, S. *Hyperfine Interaction* **1990**, *53,* 391.
(38) de Tacconi, N. R.; Rajeshwar, K.; Lezna, R. O. *J. Electroanal. Chem.* **2001**, *500*, 270.
(39) Bharathi, S.; Nogami, M.; Ikeda, S. *Langmuir* **2001**, *17*, 7468.
(40) Pyrasch, M.; Toutianoush, A.; Jin, W.; Schnepf, J.; Tieke, B. *Chem. Mater.* **2003,** *15*, 245.
(41) Pyrasch, M.; Tieke, B. *Langmuir* **2002**, *17*, 7706.
(42) Torres, G. R.; Agricole, B.; Delhaes, P.; Mingotaud, C. *Chem Mater.* **2002**, *14*, 4012.
(43) Zhan, P.; Xue, D.; Luo, H.; Chen, X. *Nano Lett.* **2002**, *2*, 845.
(44) Rajeshwar, K.; de Tacconi, N. R.; Chenthamarakshan, C. R. *Chem. Mater.* **2001**, *13*, 2765. See also references therein.
(45) Vaucher, S.; Fielden, J. ; Li, M.; Dujardin, E.; Mann, S. *Nano Lett.* **2002**, *2*, 225.
(46) Nishizawa, M.; Kuwabata, S.; Yoneyama, H. *J. Electrochem. Soc.* **1996**, *143*, 3462.
(47) De Berry, D. W.; Viehbeck, A. *J. Electrochem. Soc.* **1983**, *130*, 249.
(48) Ziegler, J. P.; Hemminger, J. C. *J. Electrochem. Soc.* **1987**, *134*, 358.
(49) Viehbeck, A.; De Berry, D. W. *J. Electrochem. Soc.* **1985**, *132*, 1369.
(50) Ziegler, J. P.; Lesniewski, E. K.; Hemminger, J.C. *J. Appl. Phys.* **1987**, *61*, 3099.
(51) Gruszecki, T.; Holmström, B. *J. Appl. Electrochem.* **1991**, *21*, 430.
(52) de Tacconi, N. R.; Carmona, J.; Rajeshwar, K. *J. Phys. Chem. B* **1997**, *101*, 10151.
(53) de Tacconi, N. R.; Carmona, J. ; Balsam, W. L.; Rajeshwar, K. *Chem. Mater.* **1998**, *10*, 25.
(54) de Tacconi, N. R. ; Rajeshwar, K.; Lezna, R. O. *Electrochim. Acta* **2000**, *45,* 3403.
(55) Kulesza, P. J.; Faszynska, M. *J. Electroanal. Chem.* **1988**, *252*, 461.
(56) Kulesza, P. J.; Faszynska, M. *Electrochim. Acta* **1989**, *34*, 1749.
(57) Joseph, J.; Gomathi, H.; Prabhakara Rao, G. *J. Electroanal. Chem.* **1991**, *304*, 263.
(58) Zaldivar, G. A. P.; Grushikem, Y.; Benvenutti, E. V.; de Castro, S. C.; Vasquez, A. *Electrochim. Acta* **1994**, *39*, 33.
(59) Chen, S-M. *J. Electroanal. Chem.* **2002**, *521*, 29.
(60) Kulesza, P. J.; Malik, M. A.; Zamponi, S.; Berrettoni, M.; Marassi, R. *J. Electroanal. Chem.* **1995**, *397*, 287.
(61) Murray, R. W. in *Electroanalytical Chemistry*, Bard, A. J., Ed., Marcel Dekker: New York, 1984; Vol. 13, p. 191.
(62) Doblhofer, K.; Rajeshwar, K. in *Handbook of Conducting Polymers*, Skotheim, T.A.; Elsenbaumer, R. L.; Reynolds, J. R., Eds., Marcel Dekker: New York, 1998; Ch. 20, pp. 531-588.
(63) Bocarsly, A. B.; Sinha, S. *J. Electroanal. Chem.* **1982**, *140*, 167.

(64) Siperko, L. M.; Kuwana, T. *Electrochim. Acta*, **1987**, *32*, 765.
(65) Engel, D.; Grabner, E. W. *Ber. Bunsenges. Phys. Chem.* **1985**, *89*, 982.
(66) Gao, Z.; Wang, G.; Li, P.; Zhao, Z. *Electrochim. Acta* **1991**, *36*, 147.
(67) Malik, M. A.; Horanyi, G.; Kulesza, P. J.; Inzelt, G.; Kertesz, V.; Schmidt, R.; Czirok, E. *J. Electroanal. Chem.* **1998**, *452*, 57.
(68) de Tacconi, N. R.; Rajeshwar, K. unpublished data, 2001-2002.
(69) Kulesza, P. J.; Malik, M. A.; Berrettoni, M.; Giorgetti, M.; Zamponi, S.; Schmidt, R.; Marassi, R. *J. Phys. Chem. B* **1998**, *102*, 1870.
(70) Jin, Z.; Dong, S. *Electrochim. Acta* **1990**, *35*, 1057.
(71) Ho, K-C.; Chen, J-C. *J. Electrochem. Soc.* **1998**, *145*, 2334.
(72) Jiang, M.; Zhou, M.; Zhao, *Z. Ber. Bunsenges. Phys. Chem.* **1991**, *95*, 720.
(73) Lasky, S. J.; Buttry, D. A. *J. Am. Chem. Soc.* **1988**, *110*, 6258.
(74) Csahck, E.; Vieil, E.; Inzelt, G. *J. Electroanal. Chem.* **1998**, *457*, 251.
(75) Haight, S. M.; Schwartz, D. J.; Lilga, M. A. *J. Electrochem. Soc.* **1999**, *146*, 1866.
(76) Ochs, S.; Grabner, E. W.; Mohler, E. *Ber. Bunsenges. Phys. Chem.* **1996**, *100*, 594.
(77) Kuwana, T.; Heineman, W. R. *Acc. Chem. Res.* **1976**, *9*, 241.
(78) Kuwana, T.; Winograd, N. in *Electroanalytical Chemistry*, Bard, A. J., Ed., Marcel Dekker: New York, 1974; Vol. 7, Chap. 1.
(79) Heineman, W. R.; Hawkridge, F. M.; Blount, H. N. in *Electroanalytical Chemistry*, Bard, A. J., Ed., Marcel Dekker: New York, 1984; Vol. 13, Chap. 1.
(80) Heineman, W. R. *J. Chem. Educ.* **1983**, *60*, 305. See also references therein.
(81) Gale, R. J., Ed., *Spectroelectrochemistry: Theory and Practice*, Plenum: New York, 1988.
(82) Rajeshwar, K.; Lezna, R. O.; de Tacconi, N. R. *Anal. Chem*. **1992**, *64*, 429 A.
(83) Ghosh, S. N. *J. Inorg. Nucl. Chem.* **1974**, *36*, 2465.
(84) Hester, R. E.; Nour, E. M. *J. Chem. Soc., Dalton Trans.* **1981**, 938.
(85) Nakamoto, K. *Infrared and Raman Spectra of Inorganic and Coordination Compounds*, John Wiley: New York, 5th ed., 1997.
(86) Zhang, H-Q.; Lin, X-Q. *Talanta* **1997**, *44*, 2069.
(87) Arancibia, V.; Beden, B.; Leger, J-M.; de Tacconi, N. R.; Lezna, R. O. in *Molecular Functions of Electroactive Thin Films*, Oyama, N.; Birss, V., Eds., The Electrochemical Society: Pennington, New Jersey; 1998, Proceedings Volume 98-26, pp. 114-119.
(88) Lezna, R. O.; Romagnoli, R.; de Tacconi, N. R.; Rajeshwar, K. *J. Electroanal. Chem*. **2003**, *544*, 101.
(89) Humphrey, B. D.; Sinha, S.; Bocarsly, A. B. *J. Phys. Chem.* **1984**, *88*, 736.
(90) Son, Y.; Rajeshwar, K. *J. Chem. Soc. Faraday Trans.* **1992**, *88*, 605.
(91) Kulesza, P. J.; Zamponi, S.; Malik M. A.; Berrettoni, M.; Wolkiewicz, A., Marassi, R. *Electrochim. Acta* **1998**, *43*, 919.
(92) De Angelis, T. P.; Heineman, W. R. *J. Chem. Educ.* **1976**, *53*, 594.
(93) Lezna, R. O.; de Tacconi, N. R.; Rapallini, J. A.; Arvia, A. J. *An. Asoc. Quim. Argent.* **1988**, *76*, 25.
(94) Juanto, S.; Lezna, R. O. Arvia, A. J. *Electrochim. Acta* **1994**, *39*, 81.
(95) Lezna, R. O.; Juanto, S.; Zagal, J. H. *J. Electroanal. Chem.* **1995**, *389*, 197.
(96) Sato, O.; Einaga, Y.; Fujishima, A.; Hashimoto, K. *Inorg. Chem.* **1999**, *38*, 4405.

(97) Bleuzen, A.; Lomenech, C; Escax, V.; Villain, F.; Varret, F.; Cartier dit Moulin, Ch.; Verdaguer, M. *J. Am. Chem. Soc.* **2000**, *122*, 6648.
(98) Parish, R. V. *The Metallic Elements*, Longman: London and New York, 1977; p.76.